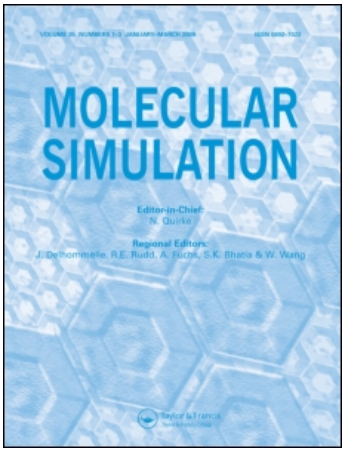

Molecular Simulation
Publication details, including instructions for authors and subscription information:
http://www.informaworld.com/smpp/title~content=t713644482

Interfacial Tension Behaviour of Water/Hydrocarbon Liquid-Liquid Interfaces: A Molecular Dynamics Simulation

M. Natália D.S.Cordeiro

Online publication date: 13 May 2010

To cite this Article D.S.Cordeiro, M. Natália(2003) 'Interfacial Tension Behaviour of Water/Hydrocarbon Liquid-Liquid Interfaces: A Molecular Dynamics Simulation', Molecular Simulation, 29: 12, 817 — 827
To link to this Article: DOI: 10.1080/0892702031000121905
URL: http://dx.doi.org/10.1080/0892702031000121905

Molecular Simulation, VOL. 29 (12), December 2003, pp. 817–827

Taylor & Francis
Taylor & Francis Group

Interfacial Tension Behaviour of Water/Hydrocarbon Liquid–Liquid Interfaces: A Molecular Dynamics Simulation

M. NATÁLIA D.S.CORDEIRO*

CEQUP/Departamento de Química, Faculdade de Ciências, Universidade do Porto, Rua do Campo Alegre, 687, 4169-007 Porto, Portugal

(Received October 2002; In final form January 2003)

Molecular dynamics simulations of the water–isooctane interface are performed to sort out the effect of temperature on the properties of liquid–liquid interfaces. Reliable interaction potential models are applied to describe the interactions, including the treatment of long-range electrostatic forces. It is shown that the increase in temperature has little effect on the basic structural features of the interface, i.e. its sharpness and corrugation. Other interfacial properties, such as the density profile, specific solvent orientations or hydrogen-bonding characteristics are nearly identical for the range of temperatures considered (from 277 to 323 K). However, the liquid–liquid interfacial tension of the water/isooctane system has a non-monotonic behaviour, presenting a maximum at a specific temperature, in contrast to the monotonic decay found for the liquid–vapour case. This behaviour is similar to the one observed for binary mixtures of partially miscible Lennard–Jones fluids.

Keywords: Liquid–liquid interfaces; Interfacial tension; Molecular dynamics simulations; Temperature dependence

INTRODUCTION

The study of liquid–liquid interfaces is essential for understanding many chemical and biological processes as well as several technological applications. Ion transfers between two electrolyte solutions, phase-transfer catalysis, or drug delivery to cells are some of such processes that have received much attention lately [1–4]. Besides this, there is an inherent fundamental interest in the study of liquid interfaces, since they are characterized by a set of unique properties, which are expected to influence the behaviour and chemical reactivity of solutes in a way markedly different from that of bulk liquid or gas-phase.

A detailed knowledge of the structural properties of the liquid–liquid interface such as surface roughness, density profiles and, especially, interfacial tension behaviour is crucial to the problem. Due to its nature as a buried interface, very few experimental techniques can directly probe the molecular detailed picture of such an interface. Nevertheless, recent experimental techniques like vibrational sum frequency spectroscopy [5,6] and X-ray [7,8] and neutron reflectance [9] have given useful insights into the structure and dynamics of these interfacial systems. On the other hand, Monte Carlo [10,11] and Molecular Dynamics (MD) simulations [12–31] provide information on the interfacial microscopic structure with greater detail than is experimentally accessible.

In particular, recently, Díaz-Herrera and coworkers [25] have studied the density profile and interfacial tension of a binary mixture of practically immiscible fluids using MD simulations. They showed that, for this fluid mixture, the interfacial tension as a function of temperature can have a maximum, unlike the monotonous temperature dependence in the liquid–vapour case. However, these authors have resorted to a very simple model fluid which did not include any intramolecular degrees of freedom.

With the purpose of getting a more thorough description of the effect of temperature on the thermodynamic and structural properties of liquid interfaces, MD equilibrium simulations of the water/isooctane (ISOC) system have been performed for temperatures in the range 277–323 K.

*Fax: +351-226082959. E-mail: ncordeir@fc.up.pt

ISSN 0892-7022 print/ISSN 1029-0435 online © 2003 Taylor & Francis Ltd
DOI: 10.1080/0892702031000121905

The present work complements previous results obtained in our group for this interfacial system at $T = 298\,K$ [27]. The remainder of the paper is organized as follows: in the second section, the molecular model and potential functions used for both ISOC and water are outlined, together with the details of the simulations. The third section reports the results obtained in this study, along with an analysis of the structural properties of both solvents near and away from the interface for the different temperatures. The interfacial tension is calculated by the fluctuations of the interfacial profile according to capillary wave theory, and its behaviour is discussed. Finally, some concluding remarks and future developments of this work are presented in the last section.

SYSTEMS AND METHODS

The intermolecular potentials consisted of pairwise additive interactions between sites, centres of spherically symmetrical Lennard–Jones (LJ) potentials that carried partial charges. For the water molecules, a rigid three-site model is used with the partial charges and LJ parameters of the SPC/E potential [32]. This potential has been shown to properly reproduce the bulk and interfacial properties of water [33–34]. Each ISOC molecule is represented by an eight-atom interaction site model in which united atoms of mass 13, 14 and 15 replace the CH, CH_2 and CH_3 groups, respectively. Being a saturated hydrocarbon, the ISOC intermolecular potential contains LJ terms only and its parameters are taken from the AMBER [35] force field. Finally, the interactions between the H_2O and ISOC molecules are modelled by an LJ intermolecular potential whose parameters were derived using standard geometric combination rules, i.e. $\sigma_{ij} = (\sigma_i \cdot \sigma_j)^{1/2}$ and $\varepsilon_{ij} = (\varepsilon_i \cdot \varepsilon_j)^{1/2}$.

During the MD simulations, all bond angles and dihedrals of the ISOC molecules were considered flexible and the corresponding intramolecular potential terms computed via the CHARMm [36] force field. This particular force field was chosen since previously tests [37] showed that its torsional potential is somewhat more specific than that of the AMBER force field. On the contrary, the ISOC bond lengths were fixed by means of the SHAKE algorithm [38] with a preset tolerance of 10^{-8} Å. This bond constrains along with the rigid water model render possible the increase of the time step used (up to 2 fs), thereby resulting in a better sampling of the configurational space. The absence of coupling between the water stretching and bending and the other vibrations of the system justifies this procedure. Also, preliminary checks confirmed that it has no effect on the properties studied here [26,27].

The water/isooctane liquid–liquid interface was investigated at three different thermodynamic conditions, wherein the temperature was varied (277, 298 and 323 K) and the pressure fixed (1 bar). In all the simulations, the desired temperature and pressure were maintained using the Nosé-Hoover thermostat and barostat [39,40]. The interface was modelled by a system containing 794 water molecules and 168 ISOC molecules filling a box of cross section of $25 \times 25\,Å^2$. Firstly, the two bulk phases were set up independently by equilibrating the liquids in two separate boxes with the same cross section and a length (along the z axis) that mimics the experimental pure liquids' bulk density (respectively, $0.997\,g/cm^3$ for water and $0.698\,g/cm^3$ for ISOC). At 298 K and 1 bar, simulation runs of 300 ps were found enough to guarantee that all energetic properties, pressure and volume were stabilized and oscillating around a mean value. The two boxes were then brought together into one single box with the same cross section (from now on, the $x{\cdot}y$ plane), and the water phase translated in the z direction up to the centre of this box. The interactions between molecules of both liquids were slowly switched on during a run of 10 ps, which was followed by an equilibration run of 300 ps at constant volume and temperature. A further equilibration of the interfacial system proceeded in the NPT ensemble for 450 ps. The last configuration of the 450 ps run (298 K) was then used as the starting configuration for the simulations at 277 and 323 K. Trajectories of 600 and 400 ps were adequate for equilibrating the system at these new temperatures according to the criteria mentioned before.

All production simulations were carried out in the NPT ensemble to enable volume variations. Notice that if the initial volume was fixed, as the interface density is unknown *a priori*, it might induce serious restrictions in the formation of the interface. At 277 and 298 K, production runs of 700 ps were performed for data collection, while at 323 K a longer run of 1100 ps was used. Average properties were accumulated from values computed every 10 time-step iterations and their fluctuations estimated by the variation in block averages.

The MD simulations were carried out using the DL_POLY program [41]. This program solves the equation of motions using a Verlet leapfrog algorithm. For the reasons stated above, a time step of 2 fs was employed. Periodic boundary conditions were applied in all three directions, giving rise to two interfaces. Care was especially taken to corroborate that the system size provided enough separation to preclude interfacial correlations. The Ewald summation method with tinfoil boundary conditions was applied to deal with long-range electrostatic forces. The real part of the Ewald sum and the LJ

interactions were truncated at a molecular separation of 12.25 and 10 Å, respectively. The forces between pairs of sites at distances larger than 10 Å were evaluated by a multiple time step algorithm [42] with an integration step of 16 fs. It has been checked that good energy conservation (without thermostat) is achieved with this algorithm, and the system properties are unaffected by its use [26–29].

RESULTS AND DISCUSSION

Interfacial Width and Position

A clear insight into the density fluctuations at the interface can be obtained from the probability distributions of the local interface width and position. By analyzing these distributions as a function of the interface's subdivision, local surface deformations can be characterized that would otherwise be impossible to differentiate in calculations of properties such as the density profile.

As has been done in previous studies [10,15,22,26,30], the interfacial plane is first divided into $N \times N$ square units with a minimum side length not smaller than the bulk correlation length (ξ_b). The highest N must be such that $S^{1/2}/N > \xi_b$, where S is the total surface area and ξ_b is of the order of a molecular length (about 6.5 Å for ISOC). Then, the local interfacial width (w_{ij}) and position (h_{ij}) are defined as follows:

$$w_{ij}^{\text{left}} = (\max(z_{ij}^{\text{ISOC}}) - \min(z_{ij}^{\text{H}_2\text{O}})) \tag{1a}$$

$$h_{ij}^{\text{left}} = \frac{1}{2}(\min(z_{ij}^{\text{H}_2\text{O}}) + \max(z_{ij}^{\text{ISOC}})) \tag{2a}$$

$$w_{ij}^{\text{right}} = (\max(z_{ij}^{\text{H}_2\text{O}}) - \min(z_{ij}^{\text{ISOC}})) \tag{1b}$$

$$h_{ij}^{\text{right}} = \frac{1}{2}(\max(z_{ij}^{\text{H}_2\text{O}}) + \min(z_{ij}^{\text{ISOC}})) \tag{2b}$$

where $\max(z_{ij}^{\text{ISOC}})$ is the highest z-coordinate of the ISOC molecules in each subunit from the left side of the simulation box, and $\min(z_{ij}^{\text{H}_2\text{O}})$ is defined analogously. As can be seen, the local width and position for the right interface are defined by simply replacing the maximum z-coordinate by the minimum z-coordinate and vice-versa.

The resulting probability distributions, $p(w_{ij})$ and $p(h_{ij})$, of the water/ISOC system at 323 K are displayed in Fig. 1 for several choices of N. Notice that data coming from both interfaces was accumulated to improve the statistics. Notice also that $N = 1$ denotes the entire interface, while in $N = 4$ each subunit corresponds to 1/16 of the interfacial area.

Figure 1 shows that, as N increases, the peak and the average of the width distribution are shifted towards negative values. Specifically, the average interface width goes from 3.9 for $N = 1$ to 1.8, 0.01 and -1.2 for $N = 2$, 3 and 4, respectively. On the other hand, the position distributions are centred at about the same average value (19.0–19.1 Å), but become broader as N grows. These plots are consistent with a picture of a very sharp interface without significant mixing, but which is highly corrugated by capillary waves. At this temperature (323 K), those waves can reach up to 4 Å onto either phase. Note that if the interface was molecularly diffuse and characterized by a gradual change in concentration, $p(w_{ij})$ would be centred at some large positive value independently of N. Also, for a flat uncorrugated interface, $p(h_{ij})$ would be independent of N.

These probability distributions were only shown for the highest temperature considered as they were identical for the other temperatures (just more sharper). Thus, judging from the present results, one may conclude that the basic structural characteristics of the water/ISOC interface (i.e. its sharpness and corrugation) seem to be preserved for a reasonable range of temperatures.

Density Profiles

The average density profiles of water and ISOC as a function of the distance to the interface are shown in Fig. 2 for the three studied temperatures. These profiles are obtained by computing the liquid densities in slabs of 0.5 Å, parallel to the x–y interfacial plane, and accumulating data from the two interfaces. In particular, they take into account the dynamical local instantaneous position of the interface: they correspond to a time average over the $N \times N$ subunits ($N = 4$) considering, within each subunit, the position of the interface as $\max(z_{ij}^{\text{ISOC}})$ (or $\min(z_{ij}^{\text{ISOC}})$) for the water phase and as $\min(z_{ij}^{\text{H}_2\text{O}})$ (or $\max(z_{ij}^{\text{H}_2\text{O}})$) for the ISOC phase. This approach has been used before [27,30] and has been shown to provide a more correct description of properties that depend on the interfacial position.

As clearly seen in Fig. 2, the water/ISOC system forms a stable, well-defined interface at all thermodynamic conditions, thus indicating that the potential model chosen successfully describes the formation of the interface. The bulk ISOC and H_2O are also well separated and their estimated average densities are in good agreement with the experimental values. For $T = 298$ K, the average water density computed by selecting a 20 Å thick layer, 15 Å away from the interface, is 0.972 g/cm^3 (i.e. the density of the SPC/E water model [32]) and that of ISOC corresponding to an equal layer, but in this case 20 Å away from the interface, is 0.714 g/cm^3 which is quite close to the experimental value of 0.698 g/cm^3 [43].

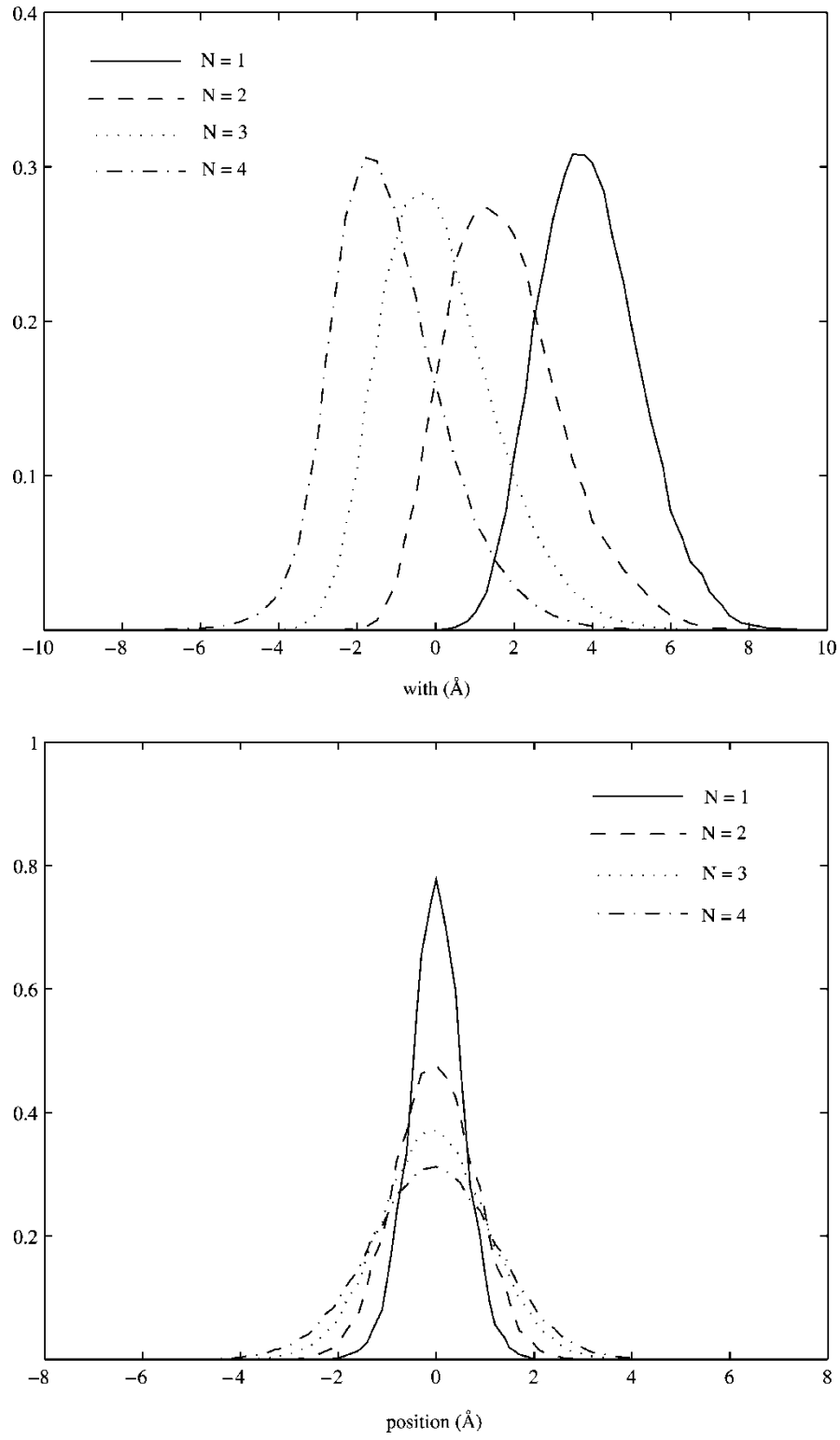

FIGURE 1 Probability distribution functions for the with (top) and position (bottom) of the water/isooctane liquid–liquid interface at 323 K. (See text for details.).

For all profiles of Fig. 2, density maxima appear in both sides of the interface denoting a strong layering of both liquids. At all temperatures, there are 2–3 distinct peaks in the ISOC profile and 1–2 peaks in the water profile, corresponding to definite packed layers of the liquids at (and past) the interface. This packing effect propagates more deeply into the bulk ISOC phase than into the water phase. The visible layering structure of the interface thus reminds that of a density distribution at a wall, like in solid–liquid

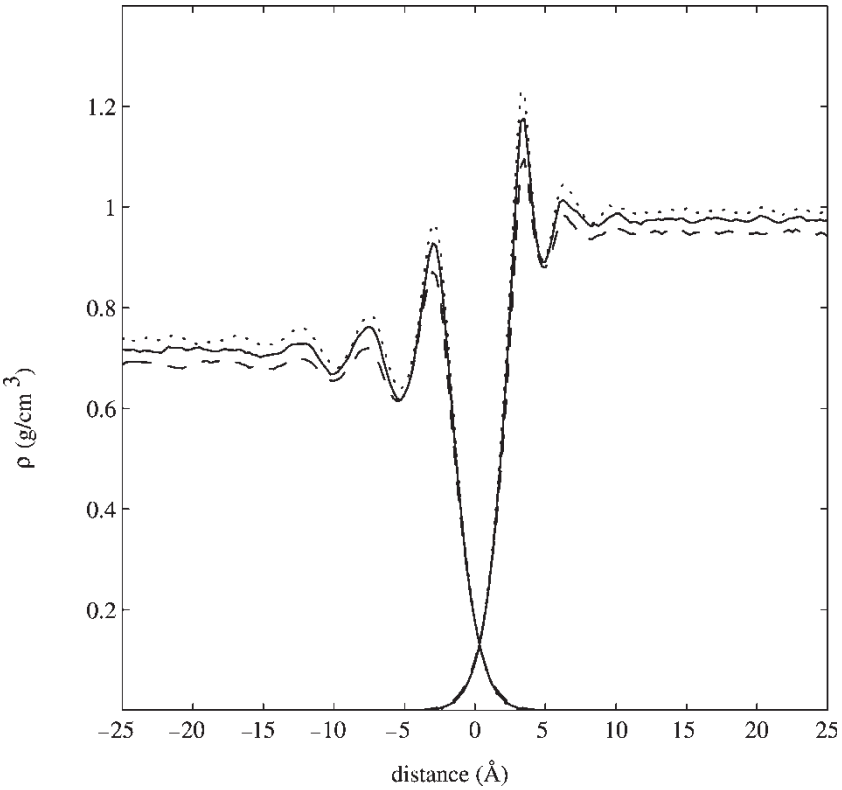

FIGURE 2 Average density profile of the H_2O/ISOC system at various temperatures, calculated using a dynamical local definition of the interface. The dotted line corresponds to $T = 277$ K, the solid line to $T = 298$ K, and the dashed line to $T = 323$ K.

interfacial systems [44–47]. Similar results have been reported at $T = 298$ K for water close to much more hydrophilic liquids such as liquid 2-heptanone which is the hydrophilic analogue of ISOC [26].

To consider temperature effects, plots of reduced density (ρ/ρ^{bulk}) as a function to the distance to the interface have been analysed (data not shown); they reveal that the local density enhancements decrease for both liquids as the temperature raises. At the interface, they are similar between $T = 277$ and 298 K, but are much higher for water than for ISOC on going from $T = 298$ to 323 K. Temperature also has an effect on the liquids' coexistence region, as can be seen by examining the crossed decay of the density of both liquids near the interface (Fig. 2). The three lines in this figure are almost coincident but a finer analysis shows that the coexistence region grows with increasing temperature (especially at $T = 323$ K). Thus, heating up the system, as the liquids are completely demixed, does not change the composition of the bulk phases but reflects only in decreasing oscillations and to an expansion of the interface region.

Bulk and Interfacial Structure

In the following, the effect of temperature on the structural properties of the water/ISOC system at the interface and in bulk regions will be analysed in terms of the orientation distributions of both ISOC and H_2O molecules and the hydrogen-bonding patterns (HB) of the aqueous phase. Atomic radial distribution functions (RDF) for both liquids have also been computed but they are not shown, as they do not provide extra features to the results discussed below.

Isooctane

In order to characterize the structure of the interfacial isooctane, the orientational probability distribution for the angle between the molecular axis of ISOC and the normal to the interface was computed for the three different temperatures. Figure 3 shows only this distribution for $T = 323$ K, but the general patterns are identical for the two other temperatures. Nevertheless, in the same figure, the ISOC orientational distributions are plotted for all temperatures at two specific regions, namely at the interface and in the bulk. Each region corresponds to a slab of 6 Å thickness, i.e. roughly the size of the ISOC molecule. Notice that both plots in Fig. 3 display the results averaged for the two interfaces.

For all temperatures, the ISOC molecules tend to lie parallel to the interfacial plane and this orientational order is mainly restricted to the first molecular layer into bulk ISOC, after which an isotropic

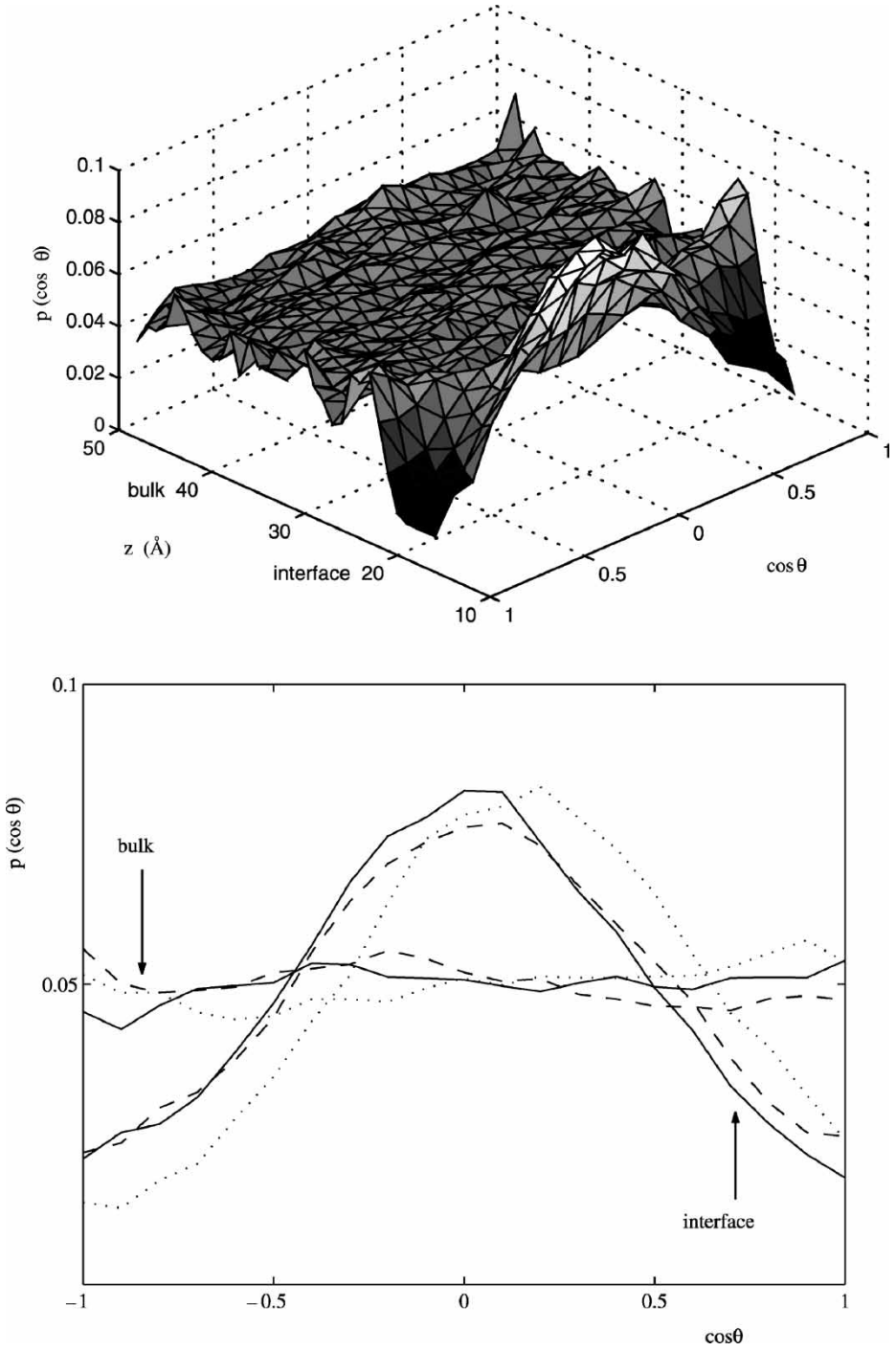

FIGURE 3 Isooctane orientational probability distribution as a function of the distance to the interface. θ is the angle between the isooctane molecular axis and the normal to the interface. The top panel shows the results obtained for the H_2O/ISOC system at 323 K. The bottom panel compares the nonane orientation at specific regions—in the bulk and at the interface—for the various temperatures (dotted line: $T = 277$ K; solid line: $T = 298$ K, and dashed line: $T = 323$ K). Each curve in this panel corresponds to a probability for a 6 Å layer.

distribution is reached. One should remark that the curves pertaining to the interface and bulk regions (bottom panel) are quite noisier due to the smaller number of molecules used to compute the averages (even in the bulk). They point out to a similar equal extent orientation distributions at the interface, although at $T = 277$ K the maximum is slightly shifted (to an angle of $\approx 80°$), but this might result from statistical noise.

Water

One unique point about water is that H_2O molecules can form hydrogen bonds to each other. By looking at

the average number of H-bonds per water molecule (NHB) as a function of the distance to the interface, one can infer how the bulk-interface transition changes the water structure. Here, two water molecules are considered to be H-bonded if their intermolecular O–H distance is less than 2.4 Å (i.e. the position of the first minimum of the O–H RDF). Other definitions are possible (e.g. based on an energetic criterion) but the results seem to be independent from the exact definition [15]. One can also compute the average number of neighbours in the water coordination shell (NNS), which is defined by the first minimum of the O–O RDF (3.5 Å). However, the most interesting quantity to estimate the degree of H-bonding is the percentage of water molecules within the first coordination shell that are H-bonded (%HB = (NHB/NNS) × 100). In Fig. 4, both quantities are shown for the water/ISOC system at all temperatures investigated.

All MD simulations up to date that studied the H-bonding patterns at water/organic interfaces suggest that the degree of H-bonding is reinforced near the interface, regardless the hydrophobic nature of the organic phase [10,17,22,26,30]. This is that although the NNB and NNS decrease at the interface with respect to the bulk, the %HB increases. A similar trend is found here for all temperatures and, as seen in Fig. 4, the curves run parallel to each other just reflecting the variations in water density.

Further insight into the water's structural changes induced by the interface can be obtained by examining the orientation distribution of the water dipoles. In fact, it is now well-known that H_2O molecules display a certain orientational order at the liquid–vapour interface [48] or other liquid–liquid interfaces due to their directional interactions [10,15,17,26,30].

Figure 5 displays the probability distribution for the angle between the H_2O dipole moment and the interface normal for the water/ISOC system at $T = 323$ K. Again the system exhibits nearly identical behaviour at the other temperatures. As before, the water orientational distributions are compared at two specific regions (at the interface and in the bulk) for $T = 277$, 298 and 323 K. The regions are defined as explained in the last section, but now they have a width of 4 Å.

One can observe in Fig. 5 the typical behaviour of water near a hydrophobic interface. The water dipole orientation goes from isotropic (in bulk) to lying preferentially parallel to the interface (at the interface), and this preferential orientation is limited to a few molecular layers away from the interface. The relatively weaker orientational order of water compared to that of ISOC (see Figs. 3 and 5) certainly results from the rather different molecular symmetry of both molecules. One may also observe that, as the temperature increases, the distribution of the water dipoles at the interface become broader, especially at the highest temperature.

Finally, it should be noticed that all computed intermolecular RDFs do not reveal any specific solvation between water and the ISOC molecules for this range of temperatures.

Interfacial Tension

The interfacial tension —$\gamma(T)$— can be calculated by means of the mechanical definition using the components of the pressure tensor [49]. $\gamma(T)$ can also be determined through the calculation of the width of the interface. By treating thermal fluctuations according to the capillary wave theory, one gets the following relationship between the width due to capillary broadening and the surface tension [49]:

$$\sigma^2 = \frac{k_B T}{2\pi\gamma} \ln\left(\frac{L}{\xi_b}\right) \tag{3}$$

where k_B is the Boltzmann constant, T is the absolute temperature, and L and ξ_b are the upper and lower wavelength limits. L and ξ_b are determined by the size along the x or y dimension of the box and the bulk correlation length.

Previous studies of liquid–liquid interfaces have demonstrated that both methods give quite close results [30,31] and, here, the capillary wave theory has been applied. Thus, the interfacial tension was estimated according to Eq. (3), by taking σ^2 from the $p(h_{ij})$ distribution with the highest $N(=4)$, $\xi_b = 6.5$ Å and $L = L_x$. Table I summarizes the results obtained for the water/ISOC system at the three temperatures. The calculated value for 298 K −58.8 dyn/cm— reasonably agrees with the experimental reported value (50.1 dyn/cm) [50]. Notice that this value is slightly larger than the one attained in our previous MD simulations using the SPC water model (54.4 dyn/cm) [27].

The most noteworthy feature in Table I is, however, the non-monotonic behaviour of $\gamma(T)$ for this range of temperatures, i.e. the maximum observed at $T = 298$ K. This behaviour differs from the monotonous temperature dependence found in the liquid–vapour phase [52]. It might be explained as follows: increasing the temperature raises the potential energy of the system leading to an increase of $\gamma(T)$, until at $T > 298$ K, the entropic contribution drops it down. According to the results of the previous sections, the structural changes induced by the increase of temperature occur mainly in the bulk water phase, i.e. the liquid with greater mobility (less entropic price) going from bulk to the denser interfacial region, and they are more important at $T = 323$ K (see also Table I). Therefore, above $T = 298$ K, the more favourable entropic

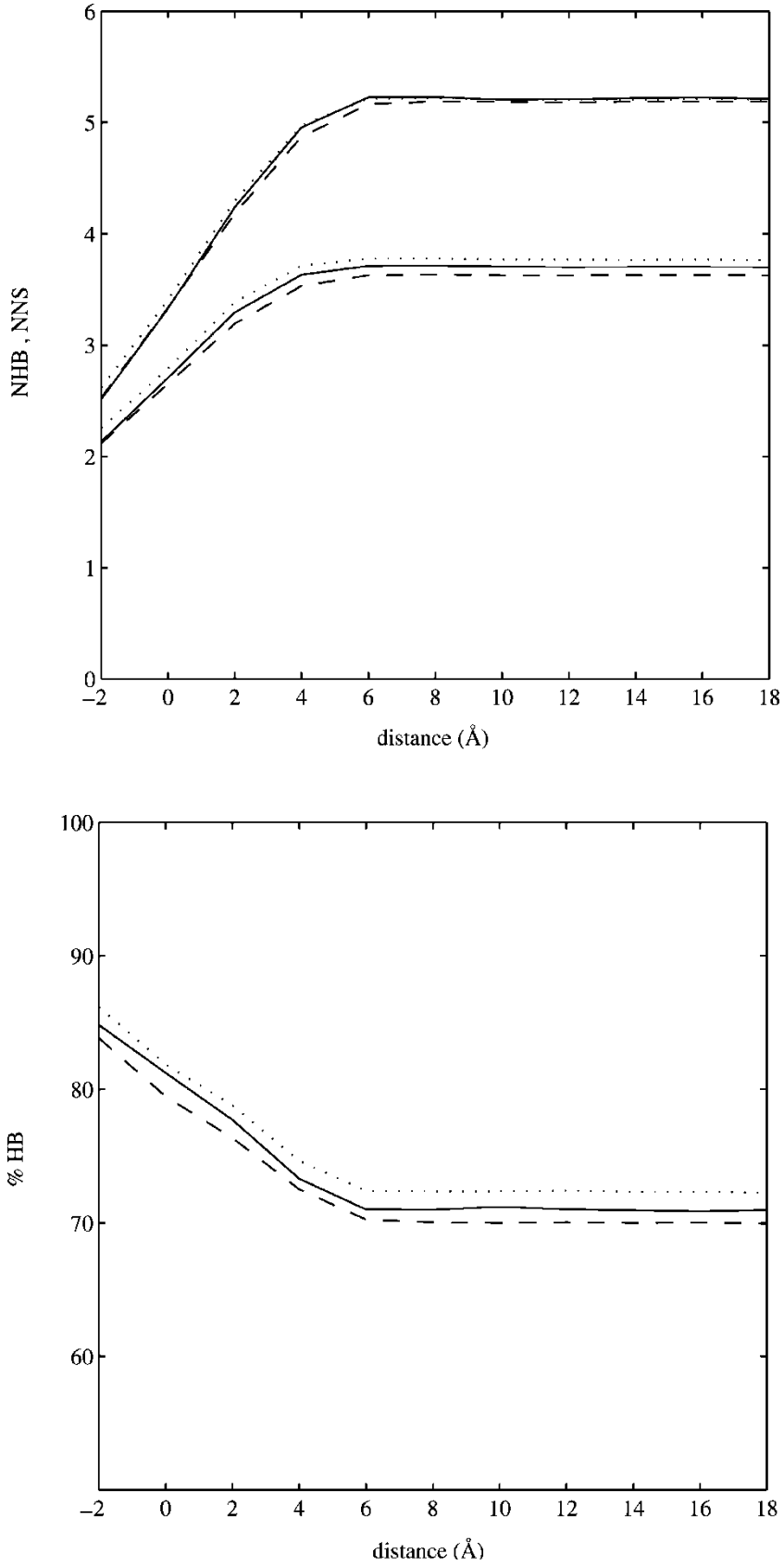

FIGURE 4 Water hydrogen-bonding characteristics for the H_2O/ISOC system at temperatures: $T = 277$ K (dotted line), $T = 298$ K (solid line) and $T = 323$ K (dashed line). Top panel shows the averaged numbers of coordinated waters (upper line) and H-bonds per water molecule (lower line) along the distance to the interface. In the bottom panel, the plot gives the percentage of water molecules inside the first coordination shell that are H-bonded. Negative distances correspond to layers into bulk ISOC and positive distances to layers into bulk H_2O.

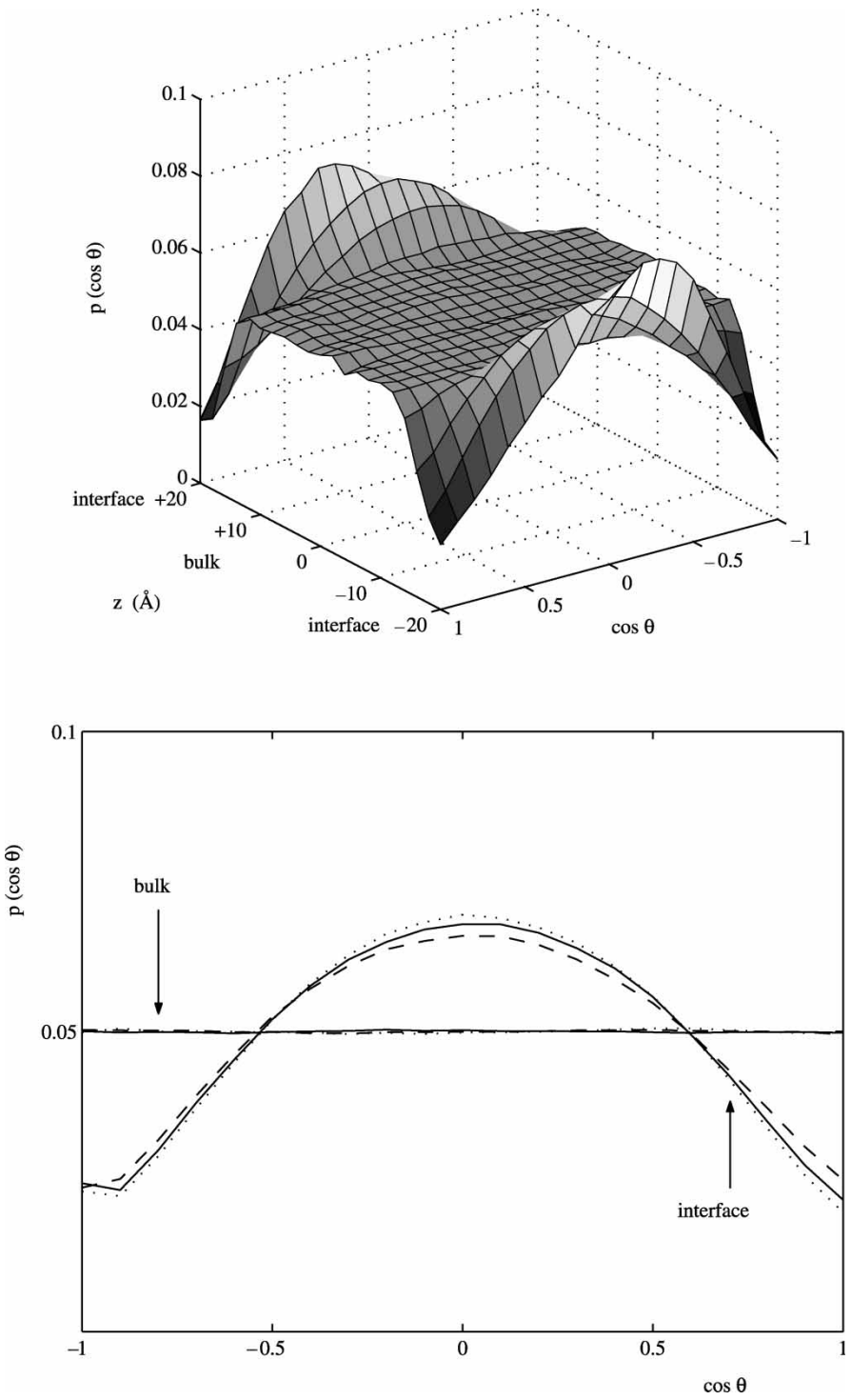

FIGURE 5 Water orientational probability distribution as a function of the distance to the interface. θ is the angle between the water dipole moment and the normal to the interface. The top panel shows the results obtained for the H_2O/ISOC system at 323 K. The bottom panel compares the water orientation at specific regions—in the bulk and at the interface—for the various temperatures (dotted line: $T = 277$ K; solid line: $T = 298$ K and dashed line: $T = 323$ K). Each curve in this panel corresponds to a probability for a 4 Å layer.

contributions should offset the more unfavourable potential energy contributions.

Recently, Song *et al.*[51] measured the interfacial tensions of several liquid–liquid water/aliphatic hydrocarbon interfaces (including n-octane) and water/aliphatic alcohol interfaces from $T = 298$ K to $T = 343$ K, at constant pressure, using the pendant drop method. The authors found that the interfacial tension of the water/aliphatic hydrocarbon systems decrease linearly with higher temperature, but those of the water/aliphatic alcohol systems first increased and then decreased with higher temperature.

TABLE I Temperature dependence of the interfacial tension for the water/isooctane liquid–liquid interface

T (K)	$\rho^{max}_{water}/\rho^{bulk}_{water}$ *	$\rho^{max}_{ISOC}/\rho^{max}_{ISOC}$ *	σ^2 (Å^2)†	γ (dyn/cm)
277	1.23	1.32	1.48	56.7 ± 0.2
298	1.21	1.30	1.52	58.8 ± 0.2
323	1.11	1.27	1.72	56.1 ± 0.2

* Values determined from the density profiles shown in Fig. 2. ρ^{max} and ρ^{bulk} correspond to the maximum and average bulk values of each profile. † Mean squared deviation of the interface position taken from the position probability distribution with $N = 4$. (See Fig. 1.).

The present results are in accord with those experimental results, at least for the range of temperatures 298–323 K.

From a theoretical point of view, the interfacial tension as a function of temperature has been investigated for binary mixtures of partially miscible LJ fluids, using MD simulations [25] and density functional theory [52]. Such studies showed that the interfacial tension of those fluid mixtures has also a maximum at a specific temperature.

These observations, allied with the fact that nearly the same structural properties are observed for water in contact with an organic phase, regardless of the nature of organic phase, certainly suggest an identical interfacial tension temperature behaviour for the interfaces between immiscible or partially miscible liquids away from critical points.

Concluding Remarks

In the present work, the equilibrium properties of the H_2O/ISOC liquid–liquid interface have been examined for states at different temperatures and constant pressure. The interactions between the different species have been described by realistic pair-additive potential models along with a proper treatment of the long-range electrostatic forces, which seems to be more important than the inclusion of many-body polarization effects in predicting the interfacial tension or other structural properties [16,22,53–54].

Perhaps the most important result of this work is the maximum observed for the interfacial tension, $\gamma(T)$, upon increasing the temperature from 277 to 323 K. Despite that, the H_2O/ISOC interface exhibits very similar gross structural features (such as surface roughness, solvent molecular orientation, and more) for the range of temperatures considered. The temperature dependence of $\gamma(T)$ for the liquid–liquid interface is thus rather different from the monotonous behaviour found for the liquid–vapour interface. This may be due to a special outbalance between the potential energy and entropy contributions to the interface free energy in the liquid–liquid case.

In the future, it is planned to extend the reported calculations to a larger fine range of temperatures. It is also interesting to speculate on the effects of changing the molecular shape of the non-polar organic liquid as well as its hydrophobicity. Judging from previous studies [25,51,52], one might anticipate that the non-monotonic behaviour of $\gamma(T)$ would prevail but its maximum would be shifted to higher temperatures for spherically shaped or more hydrophilic organic liquids. This again suggests interesting further work.

Acknowledgements

Financial support from *Fundação para a Ciência e Tecnologia* (Lisbon) through project POCTI/Qui/33765/99 is acknowledged. The author appreciates the assistance of Luis A. M. Alves and P. A. Fernandes in performing the calculations and greatly acknowledges Luis A. M. Alves for helpful discussions.

References

[1] Lipowsky, R. (1993) "Domain-induced budding of fluid membranes", *Biophys. J.* **64**, 1133.
[2] Arai, K., Ohsawa, M., Kusu, F. and Takamura, K. (1993) "Drug ion transfer across an oil–water interface and pharmacological activity", *Bioelectrochem. Bioenerg.* **31**, 65.
[3] Taniguchi, T. (1996) "Shape deformation and phase separation dynamics of two-component vesicles", *Phys. Rev. Lett.* **76**, 4444.
[4] Reymond, F., Fermín, D., Lee, H.J. and Girault, H.H. (2000) "Electrochemistry at liquid/liquid interfaces: methodology and potential applications", *Electrochim. Acta* **45**, 2647.
[5] Miranda, P.B. and Shen, Y.R. (1999) "Liquid interfaces: a study by sum-frequency vibrational spectroscopy", *J. Phys. Chem. B* **103**, 3292.
[6] Scatena, L.F., Brown, M.G. and Richmond, G.L. (2001) "Water at hydrophobic surfaces: weak hydrogen bonding and strong orientation effects", *Science* **292**, 908.
[7] Mitriniovic, D.M., Zhang, Z., Williams, S., Huang, Z. and Schlossman, M.L. (1999) "X-ray reflectivity study of the water–hexane interface", *J. Phys. Chem. B* **103**, 1779.
[8] Mitrinovic, D.M., Tikhonov, A.M., Li, M., Huang, Z. and Schlossman, M.L. (2000) "Noncapillary-wave structure at the water–alkane interface", *Phys. Rev. Lett.* **85**, 582.
[9] Bowers, J., Zarbakhsh, A., Webster, J.R.P., Hutchings, L.R. and Richards, R.W. (2001) "Neutron reflectivity studies at liquid–liquid interfaces: methodology and analysis", *Langmuir* **17**, 140.
[10] Linse, P. (1987) "Monte Carlo simulation of liquid–liquid benzene–water interface", *J. Chem. Phys.* **86**, 4177.
[11] Gao, J. and Jorgensen, W.L. (1988) "Theoretical examination of hexanol–water interfaces", *J. Phys. Chem.* **92**, 5813.
[12] Meyer, M., Mareschal, M. and Hayoun, M. (1988) "Computer modeling of a liquid–liquid interface", *J. Chem. Phys.* **89**, 1067.
[13] Carpenter, I.L. and Hehre, W.J. (1990) "A molecular dynamics study of the hexane/water interface", *J. Phys. Chem.* **94**, 531.
[14] van Buuren, A.R., Marrink, S.J., Berendsen, H.J.C. and Molecular, A. (1993) "Dynamics study of the decane/water interface", *J. Phys. Chem.* **97**, 9206.
[15] Benjamin, I. (1992) "Theoretical study of the water/1,2-dichloroethane interface: structure, dynamics and conformational equilibrium at the liquid–liquid interface", *J. Chem. Phys.* **97**, 1432.
[16] Michael, D. and Benjamin, I. (1995) "Solute orientational dynamics and surface roughness of water/hydrocarbon interfaces", *J. Phys. Chem.* **99**, 1530.

[17] Benjamin, I. (1997) "Molecular structure and dynamics at liquid–liquid interfaces", *Annu. Rev. Phys. Chem.* **48**, 407.
[18] Michael, D. and Benjamin, I. (1998) "Structure, dynamics, and electronic spectrum of N,N′-diethyl-p-nitroaniline at water interfaces", *J. Phys. Chem. B* **102**, 5145.
[19] Zhang, Y., Feller, S.E., Brooks, B.R. and Pastor, R.W. (1995) "Computer simulation of liquid/liquid interfaces. I. Theory and application to octane/water", *J. Chem. Phys.* **103**, 10252.
[20] Toxvaerd, S. and Stecki, J. (1995) "Density profiles at a planar liquid–liquid interface", *J. Chem. Phys.* **102**, 7163.
[21] Bocker, J., Gurskii, Z. and Heinzinger, K. (1996) "Structure and dynamics at the liquid mercury–water interface", *J. Phys. Chem.* **100**, 14969.
[22] Chang, T.-M. and Dang, L.X. (1996) "Molecular dynamics simulations of CCl_4–H_2O liquid–liquid interface with polariazble potential models", *J. Chem. Phys.* **104**, 6772.
[23] Dang, L.X. (1999) "Intermolecular interactions of liquid dichloromethane and equilibrium properties of liquid–vapor and liquid–liquid interfaces: a molecular dynamics study", *J. Chem. Phys.* **110**, 10113.
[24] Pohorille, A., Wilson, M.A. and Chipot, C. (1997) "Interaction of alcohols and anesthetics with the water–hexane interface. A molecular dynamics study", *Prog. Colloid Polym. Sci.* **103**, 29.
[25] Diaz-Herrera, E., Alejandre, J., Ramirez-Santiago, G. and Forstmann, F. (1999) "Interfacial tension behavior of binary and ternary mixtures of partially miscible Lennard–Jones fluids: a molecular dynamics simulation", *J. Chem. Phys.* **110**, 8084.
[26] Fernandes, P.A., Cordeiro, M.N.D.S. and Gomes, J.A.N.F. (1999) "Molecular dynamics simulation of the water/2-heptanone liquid–liquid interface", *J. Phys. Chem. B* **103**, 6290.
[27] Fernandes, P.A., Cordeiro, M.N.D.S. and Gomes, J.A.N.F. (1999) "Molecular dynamics study of the transfer of iodide across two liquid/liquid interfaces", *J. Phys. Chem. B* **103**, 8930.
[28] Fernandes, P.A., Cordeiro, M.N.D.S. and Gomes, J.A.N.F. (2000) "Influence of ion size and charge in ion transfer processes across a liquid|liquid interface", *J. Phys. Chem. B* **104**, 2278.
[29] Fernandes, P.A., Cordeiro, M.N.D.S. and Gomes, J.A.N.F. (2001) "Molecular simulation of the interface between two immiscible electrolyte solutions", *J. Phys. Chem. B* **103**, 981.
[30] da Rocha, S.R.P., Johnston, K.P., Westacott, R.E. and Rossky, P.J. (2001) "Molecular structure of the water-supercritical CO_2 interface", *J. Phys. Chem. B* **105**, 12103.
[31] Senapati, S. and Berkowitz, M.L. (2001) "Computer simulation study of the interface width of the liquid/liquid interface", *Phys. Rev. Lett.* **87**, 176101.
[32] Berendsen, H.J.C., Grigera, J.R. and Straatsma, T.P. (1987) "The missing term in effective pair potentials", *J. Phys. Chem.* **91**, 6269.
[33] Matsumoto, M., Takaoka, Y. and Kataoka, Y. (1993) "Liquid–vapor interface of water–methanol mixture. I. Computer simulation", *J. Chem. Phys.* **98**, 1464.
[34] Alejandre, J., Tildesley, D.J. and Chapela, G.A. (1995) "Molecular dynamics simulation of the orthobaric densities and surface tension of water", *J. Chem. Phys.* **102**, 4574.
[35] Pearlman, D.A., Case, D.A., Caldwell, J.W., Seibel, G.L., Singh, U.C., Weiner, P.K. and Kollman, P.A. (1991) *AMBER4* (University of California, San Francisco).
[36] Brooks, B.B., Bruccolery, R.E., Olafson, B.D., States, D.J., Swaminathan, S. and Karplus, M.J. (1983) "CHARMM: a program for macromolecular energy, minimization, and dynamics calculations", *J. Comput. Chem.* **4**, 187.
[37] Fernandes, P.A., Cordeiro, M.N.D.S. and Gomes, J.A.N.F. (1999) "Molecular dynamics simulation of liquid 2-heptanone, pure and saturated with water", *J. Phys. Chem. B* **103**, 1176.
[38] Ryckaert, J., Ciccotti, G. and Berendsen, H.J.C. (1977) "Numerical integration of the cartesian equations of motion of a system with constraints: molecular dynamics of n-alkanes", *J. Comput. Phys.* **23**, 327.
[39] Hoover, W.G. (1985) "Canonical dynamics: equilibrium phase-space distributions", *Phys. Rev.* **A31**, 1695.
[40] Melchionna, S., Ciccotti, G. and Holian, B.L. (1993) "Hoover NPT dynamics for systems varying in shape and size", *Mol. Phys.* **78**, 533.
[41] Forester, T.R. and Smith, W. (1995) *DLPOLY (version 2.6)* (Daresbury Laboratory).
[42] Forester, T.R. and Smith, W. (1996) "DL-POLY_2.0: a general-purpose parallel molecular dynamics simulation package", *J. Mol. Graph.* **14**, 136.
[43] Weast, R.C., ed (1989) *Handbook of Chemistry and Physics* (CRC Press, Boca Raton, FL).
[44] Lee, C.Y., McCammon, J.A. and Rossky, P.J. (1984) "The structure of liquid water at an extended hydrophobic surface", *J. Phys. Chem.* **80**, 4448.
[45] Heizinger, K. (1991) "Molecular dynamics studies of platinum/water interfaces", *Pure Appl. Chem.* **63**, 1733.
[46] Lee, S.H. and Rossky, P.J. (1994) "A comparison of the structure and dynamics of liquid water at hydrophobic and hydrophilic surfaces—a molecular dynamics simulation study", *J. Chem. Phys.* **100**, 3334.
[47] Schweighofer, K., Xia, X. and Berkowitz, M. (1996) "Molecular dynamics study of water next to electrified Ag(111) surfaces", *Langmuir* **12**, 3747.
[48] Wilson, M.A., Pohorille, A. and Pratt, L.R. (1988) "Surface potential of the water liquid–vapor interface", *J. Chem. Phys.* **88**, 3281.
[49] Rowlinson, J.S. and Widom, B. (1982) *Molecular Theory of Capillarity* (Clarendon, Oxford).
[50] Freitas, A.A., Quina, F.H. and Carrol, F.A. (1997) "Estimation of water–organic interfacial tensions. A linear free energy relationship analysis of interfacial adhesion", *J. Phys. Chem. B* **101**, 7488.
[51] Song, Y., Tian, Y., Xiao, Y., Ren, X. and Qiao, R. (1999) "Interfacial tensions of binary liquid–liquid systems", *Huagong Xuebao* **50**, 620 (Chinese Edition).
[52] Iatsevitch, S. and Forstmann, F. (1997) "Density profiles at liquid–vapor and liquid–liquid interfaces: an integral equation study", *J. Chem. Phys.* **107**, 6925.
[53] Motakabbir, K.A. and Berkowitz, M.L. (1991) "Liquid–vapor interface of TIP4P water: comparison between a polarizable and a nonpolarizable model", *Chem. Phys. Lett.* **176**, 61.
[54] Wallqvist, A. (1990) "Molecular-dynamics study of hydrophobic aggregation in water/methane/methanol systems", *Chem. Phys. Lett.* **165**, 437.